ELSEVIER

Chemical Engineering Journal 90 (2002) 117–129

Chemical Engineering Journal

www.elsevier.com/locate/cej

Hydrogenation kinetics of toluene on Pt/ZSM-22

Joris W. Thybaut, Mark Saeys, Guy B. Marin*

Laboratorium voor Petrochemische Techniek, Ghent University, Krijgslaan 281 (S5), B-9000 Gent, Belgium

Abstract

Kinetic experiments on the hydrogenation of toluene were performed on 0.5 wt.% Pt/ZSM-22 at temperatures in the range 423–498 K, H_2 inlet partial pressures of 100–300 kPa and toluene inlet partial pressures of 10–60 kPa. Construction of a kinetic model was based on a critical evaluation of available literature data on the hydrogenation of aromatic components together with physicochemical studies on the interaction of aromatic components and related hydrogenated products with metal surfaces as well as on quantumchemical calculations. This lead to a general kinetic model, analogous to the Horiuti Polanyi mechanism for ethylene hydrogenation, with the first four H atom addition steps not in quasi-equilibrium. Chemisorption of H_2 and toluene was assumed to occur on identical sites. No dehydrogenated surface species was taken into account. The preexponential factors were calculated using transition state theory. A model with equal surface reaction rate coefficients for the H addition steps was selected as the best model. The estimated toluene and H_2 chemisorption enthalpies amounted to -70 and $-42\,kJ\,mol^{-1}$. An activation energy in the range of 40–50 $kJ\,mol^{-1}$ was found. Under typical reaction conditions, 60% of the surface is covered by toluene and 20% by H atoms. The remaining 20% are free. Negligible amounts of partially hydrogenated species were found to be present on the catalyst surface.

Keywords: Hydrogenation; Kinetics; Toluene; Platinum; ZSM-22; Quantumchemistry

1. Introduction

The hydrogenation or saturation of aromatic components is of increasing interest due to the more stringent environmental legislation [1]. Moreover, the removal of aromatic components is beneficial for a diesel's quality as the cetane number increases with decreasing aromatic content [1,2]. In this work, the hydrogenation is approached as a part of the hydrocracking process. Extensive work has already been performed on the hydrocracking of cycloalkanes [3–5]. Reaction conditions were such that the metal catalyzed dehydrogenation reactions were in quasi-equilibrium. Since hydrogenation of aromatic species is more difficult and, hence, slower than hydrogenation of cycloalkenes, the hydrogenation equilibrium for aromatic components cannot be assumed a priori.

The hydrogenation of aromatic components has been investigated intensively. Especially in elder work benzene is used as model component [6–21]. More recently, other aromatic model components are being used, such as toluene [22–26] and xylene-isomers, ethylbenzene and naphthalene [22,27–34]. Apart from the aromatic model component, also the catalytic material plays an important role. Several metals or their combinations, such as Ni, Pt, Pd, PtPd, ... can be used. The properties of the support can also have an effect on the hydrogenation behavior [15,25,36–38]. Lin and Vannice [23,36], Chupin et al. [25] and Rousset et al. [26] have used the same combination of toluene and Pt as used in the present work.

A variety of kinetic models for the hydrogenation of aromatic model components have been proposed [13,15,22,24,27,28,30,36]. Lin and Vannice [36] considered four categories. Distinctive features between the different categories include the selection of a rate-determining step (RDS) in the hydrogenation reaction sequence or not, and the assumption of molecular H_2 or atomic H addition to the aromatic species. The final model of these authors for the hydrogenation of toluene on Pt accounts for atomic H addition to the aromatic molecule with the first H addition as the RDS. In addition, the presence of a partially dehydrogenated product as most abundant surface intermediate was incorporated to account for the formation of carbonaceous species [36].

The assumption of non-competitive chemisorption, i.e. the existence of one type of sites for H_2 chemisorption and another type of sites for the hydrocarbon chemisorption, is prevailing, but not explicitly mentioned. In recent literature [24,27,30,32], competitive chemisorption of hydrogen and the aromatic model component is explicitly dealt with and

* Corresponding author. Tel.: +32-9-264-4516; fax: +32-9-264-4999.
E-mail address: guy.marin@rug.ac.be (G.B. Marin).

1385-8947/02/$ – see front matter
PII: S1385-8947(02)00073-6

Nomenclature

A	peak surface area
$\boldsymbol{b}$	model parameter vector containing the estimated parameter values
B	benzene
CF	calibration factor
CHA	cyclohexane
CHD	cyclohexadiene
CHE	cyclohexene
F	molar flow rate (mol s^{-1})
H	enthalpy (J mol^{-1})
I	index
j	index
k	rate coefficient (mol s^{-1} $Pa^{-(m+n)}$)
k_i	rate coefficient for the ith H atom addition (s^{-1})
K_i	equilibrium coefficient of ith H atom addition
K_I	chemisorption equilibrium coefficient for species I (Pa^{-1})
m	toluene reaction order
mch	methylcyclohexane
n	H_2 reaction order
nob	number of observations
p	partial pressure (Pa)
r	reaction rate (mol $(kg\,s)^{-1}$)
R	net production rate (mol $(kg\,s)^{-1}$)
S	entropy (J mol^{-1} K^{-1})
SSQ	sum of squares
tol	toluene
W	catalyst mass (kg)
X	conversion

Greek symbols

$\boldsymbol{\beta}$	model parameter vector containing the real parameter values
θ_i	fractional surface coverage by species i

Superscripts

^	model calculated value
0	preexponential factor
comp	composite

Subscripts

0	inlet
act	activation
cat	catalyst
hyd	hydrogenation
t	total

even selected as the most likely mechanism by Lindfors et al. [24].

Apart from the above kinetic studies, other relevant information concerning the hydrogenation of aromatic components can be obtained from physicochemical studies on the interaction of aromatic species and related hydrogenated products with metal surfaces [39,41–47] or from first principles [48]. A reaction path analysis based on quantum chemical calculations allows to gain insight in the reaction mechanism and therefore the construction of a more fundamental kinetic model. Ab initio density functional calculation have been used to study, e.g. ethylene hydrogenation [48]. Most studies about aromatic components deal with benzene/CHA, however, some information on toluene/methylcyclohexane and ethylbenzene is also available [41,46]. The assumption of the first H atom (or H_2 molecule) addition as the RDS can be related to the breaking of the resonance stabilization of the aromatic species. This seems justified in the vapor phase where the standard enthalpy of formation of CHD is higher than that of benzene, CHE and CHA. On a Pt(1 1 1)-surface, however, Koel et al. [44] reported that adsorbed CHE and two adsorbed H atoms have the highest standard enthalpy of formation in the benzene hydrogenation sequence.

The present work focuses on the hydrogenation of toluene. Kinetic models are developed based on the insight gained from physicochemical studies. Other relevant information for construction of kinetic models was obtained from quantumchemical calculations. Data regression enabled the selection of a model based on statistical and physical interpretation of the results.

2. Experimental section

2.1. Catalyst and reactant

ZSM-22 loaded with 0.5 wt.% Pt was selected as the catalyst for the hydrogenation experiments. The ZSM-22 zeolite was synthesized according to a recipe described elsewhere [49], calcined, exchanged with ammonium cations, and impregnated with an aqueous solution of $Pt(NH_3)_4Cl_2$ to obtain a Pt loading of 0.5 wt.% [50]. The Pt dispersion of such a sample is 30% [51]. This low value indicates that most of the Pt metal is present as particles with a diameter of 3 nm and is located on the external surface of the zeolite crystallites since the crystal pores have only a cross-section of 0.45 nm × 0.55 nm [50]. Hence, the hydrogenation occurs in the intercrystalline pores of the zeolite. The total concentration of active sites, C_t, is calculated based on the accessible number of Pt atoms and amounts to 10^{-2} mol kg_{cat}^{-1}. Acid catalyzed conversion of hydrocarbons is limited by the shape selective character of the intracrystalline pores of the ZSM-22 zeolite [52]. Catalyst pellets were prepared by compressing the dry zeolite powder into flakes, which were crushed and sieved. Catalyst pellets with diameters between 0.8 and 1.0 mm were used in the experimental reactor. These catalyst pellets were calcined in oxygen and subsequently reduced in hydrogen at 673 K without intermittent cooling. The absence of mass transport limitations in the intercrystalline pores was verified (Weisz moduli $\sim 10^{-2}$) [53,54]. Note that intracrystalline diffusion limitations are not relevant, as the hydrogenation is localized at the external crystallite surface [50,51].

Toluene was used as model component since its hydrogenated product, methylcyclohexane, has very limited isomerization possibilities, hence, limiting possible side reactions. The use of benzene, the hydrogenated product of which has even less isomerization possibilities was rejected for an extended set of experiments regarding its carcinogenic character.

2.2. Procedures and data

2.2.1. Equipment

The kinetic data were obtained from experiments performed in a Berty reactor [55], a gas phase reactor with complete internal mixing (CSTR-type reactor). The equipment used is essentially the same as used by Steijns et al. [56]. A N_2 feed line was added to the equipment. This enabled the selection of suitable H_2 and hydrocarbon partial pressures under which reactant conversion was measurable and not transport limited at the total pressures applied. The quality of the hydrogen used (99.99%, L'Air Liquide, $H_2O + O_2$ content < 10 ppm) makes further purification of the H_2 feed unnecessary. The verification of the hydrocarbon feed flow rate is performed by monitoring the mass of the feed reservoir. Methane is used as internal standard. The equipment has a stabilization time of about 1 h, after which a sample of the reactor effluent was taken and sent on-line to the analysis section. A HP Series II 5890 GC equipped with a 50 m (i.d. = 0.25 mm) RSL-150 column with a 0.25 μm poly-dimethylsiloxane film was used. Peak identification was performed using retention indices coupled with a GC–MS system. The X-Chrom software package was used for integration of the chromatograms.

2.2.2. Data acquisition and parameter estimation

During prolonged experimental runs, i.e. 2–4 h, a slight decrease in catalytic activity was observed. Therefore, between two experiments a 10 mmol $H_2\,s^{-1}$ flow was sent through the reactor to avoid significant catalyst deactivation in the long term. The investigated range in experimental operating conditions is shown in Table 1. The variation in inlet partial pressures corresponded with molar inlet H_2 to toluene ratios from 5 to 10. The total pressure, i.e. including N_2, was in the range of 1–3 MPa. The reactant inlet partial pressure varied from 110 to 360 kPa. The total number of experiments amounted to 42.

The weight percentages of the hydrocarbon components in the reactor effluent were calculated according to

$$i\,(\text{wt.}\%) = \frac{A(i)\text{CF}(i)}{\sum_{i=1}^{n_c} A(i)\text{CF}(i)}100 \tag{1}$$

where i is the component considered, $A(i)$ the surface area on the chromatogram and $\text{CF}(i)$ its calibration factors determined according to the method proposed by Dierickx et al. [57]. This method resulted in calibration factor which were essentially the same as reported by Dietz [58]. The use of an internal standard enabled the calculation of the outlet flow rates and, hence, the verification of the carbon and mass balance over the reactor. In the further treatment of the data, the outlet flow rates were normalized to a 100% carbon balance. The total reactant conversion was calculated as

$$X = \frac{F_{\text{tol},0} - F_{\text{tol}}}{F_{\text{tol},0}} \tag{2}$$

Parameter estimations were performed using a combination of a Rosenbrock [59] and a Marquardt algorithm [60]. An in-house written code was used for the Rosenbrock method, while for the Marquardt algorithm the ordinary least square (OLS) option of the ODRPACK-package version 2.01 [61,62] was used. Some additional source code was added to ODRPACK in order to obtain additional statistical information.

The sum of squared residuals between the observed and calculated outlet flow rates of the hydrogenated product was minimized by adjusting the model parameter vector $\boldsymbol{b}$, which is expected to approach the real parameter vector $\boldsymbol{\beta}$ when the optimum is reached.

$$\text{SSQ} = \sum_{j=1}^{\text{nob}} (F_{\text{mch},j} - \hat{F}_{\text{mch},j})^2 \xrightarrow{\boldsymbol{b}} \text{minimum} \tag{3}$$

For a given kinetic model, the methylcyclohexane reactor outlet flow rate is calculated by solving the non-linear equation,

$$\hat{F}_{\text{mch},j} - \hat{R}_{\text{mch}}(T, p_t, \hat{F}_{\text{mch},j}, F^0_{\text{tol}})W_j = 0 \tag{4}$$

i.e. via the mass balance for methylcyclohexane if the latter is not fed. The calculation of the reaction rate is discussed in Section 3.

The statistical significance of the global regression was expressed by means of the so-called F-test, which is based on the comparison of the calculated sum of squares of the calculated response value and the residual sum of squares. A high F-value corresponds to a high significance of the global regression. The parameter estimates are also tested for statistical significance on the basis of their individual t-values, which are related to the sensitivity of the model calculations on the values of the individual parameters. A high t-value corresponds to a high sensitivity and, hence, a high significance or a narrow 95% approximate individual confidence interval of the corresponding parameter.

Table 1
Range of experimental conditions

Temperature (K)	Inlet H_2 pressure (kPa)	Inlet toluene pressure (kPa)	Space time ($kg_{cat}\,mol^{-1}\,s^{-1}$)	Conversion (%)
423–498	100–300	10–60	27–82	5–45

2.2.3. Quantumchemical methods

Quantumchemical calculations were performed using density functional theory [63]. Calculations were done with the Amsterdam Density Functional package [64] using self-consistent Becke Perdew (BP86) [65,66] generalized gradient (GGA) corrections to the Vosko et al. [67] LDA exchange-correlation energy. Scalar relativistic effects were included through the zero-order regular approximation (ZORA, [68]) Hamiltonian. Basis sets were of double zeta quality and constructed with slater type orbitals. The innermost atomic shells were kept frozen and replaced by an effective core potential. The extent of these frozen cores was up to and including the Pt 4f and the C 1s shell. Unrestricted DFT calculations were done and in all the computations the spin multiplicity was optimized for the lowest energy spin state. Standard SCF- and geometry-convergence criteria were applied. The Pt(1 1 1)-surface was modeled using a two-layered Pt_{22} cluster. The Pt–Pt distance was kept fixed at the bulk value of 277 pm [69]. Reactions were studied on the central atoms of this cluster. This approach was shown to yield adsorption enthalpies consistent with fully periodic slab calculations as well as experimental results for benzene [70] and 1,4-CHD [71] on Pt(1 1 1) and for various C_2H_x intermediates on Pd [72].

3. Experimental results and kinetic model

3.1. Effect of the operating conditions on the hydrogenation rate

The hydrogenation of toluene on 0.5 wt.% Pt/ZSM-22 yielded methylcyclohexane as the main product. Small amounts (<5%) of ethylcyclopentane were observed, while only trace quantities of the dimethylcyclopentane isomers were found in the reactor effluent.

The toluene hydrogenation rate showed a maximum as a function of the temperature (Fig. 1). This phenomenon has already been observed for toluene and other aromatic model components on typical hydrogenation metals, such as Pt, Pd, Ni, ... [16,19,22–24,30,31,34]. It is generally accepted that surface coverage effects are at the origin of this maximum.

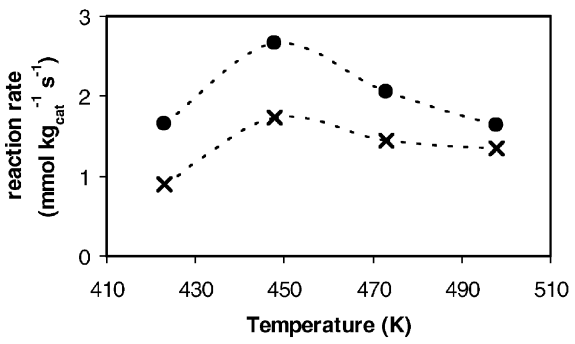

Fig. 1. Reaction rate as a function of the temperature ($p_{H_{2,0}} = 100$ kPa, $W/F_0 = 82$ kg s mol^{-1}), (●): $p_{tol,0} = 10$ kPa; (×): $p_{tol,0} = 20$ kPa.

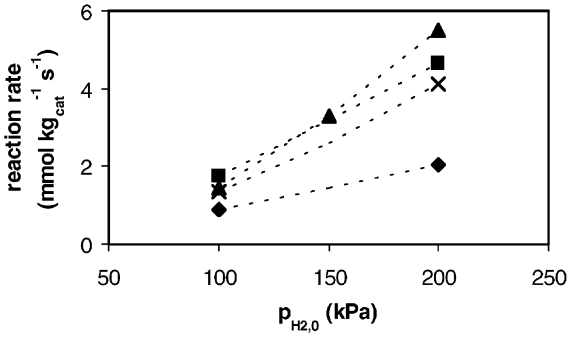

Fig. 2. Selected set of experimental data illustrating the effect of H_2 inlet partial pressure on the reaction rate ($p_{tol,0} = 20$ kPa, $W/F_0 = 82$ kg s mol^{-1}), (◆): 423 K; (■): 448 K; (▲): 473 K; (×): 498 K.

At a certain temperature, the increase of the hydrogenation rate coefficient with the temperature is overcompensated by the decrease of the surface coverage of the reaction intermediate involved in the RDS. The intrinsic character of the kinetic data has been verified, viz. Section 2.1, and hence, transport limitations cannot be invoked to explain the phenomenon. Other possible causes, such as thermodynamic limitations, catalyst poisoning or metal particle growth can be discarded [24,34].

Increasing only the H_2 inlet partial pressure and keeping all other experimental inlet variables fixed resulted in an increase of the toluene hydrogenation rate at all temperatures (Fig. 2), while an increase of only the toluene partial pressure and fixing all other inlet variables leads to a decrease of the toluene hydrogenation rate at all temperatures (Fig. 3). The partial reaction orders have been determined by a regression of all available data, i.e. not only the data presented in Figs. 2 and 3, at the temperature considered to the equation:

$$r_{hyd} = k_{hyd} p_{tol}^{m} p_{H_2}^{n} \quad (5)$$

in which m and n are the toluene and the H_2 partial reaction order, respectively. The estimated values are reported in Table 2. The H_2 partial reaction order shows an increasing trend with the temperature, in agreement with literature data [14,15,19,22–24,30]. The toluene partial reaction order is

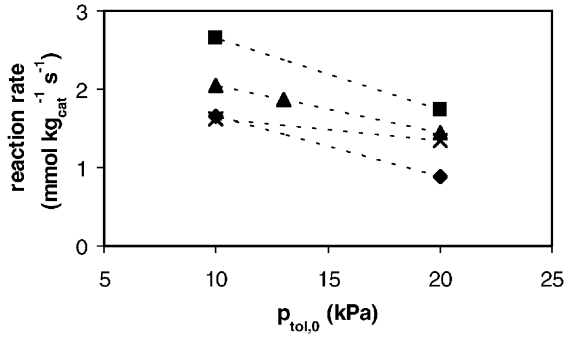

Fig. 3. Selected set of experimental data illustrating the effect of toluene inlet partial pressure on the reaction rate ($p_{H_{2,0}} = 100$ kPa, $W/F_0 = 82$ kg s mol^{-1}), (◆): 423 K; (■): 448 K; (▲): 473 K; (×): 498 K.

Table 2
H_2 and toluene partial reaction orders for the temperature range considered estimated by regression of all isothermal experimental data to Eq. (5)

Temperature (K)	m	n
423	-0.2 ± 0.1[a]	0.6 ± 0.1[a]
448	-0.2 ± 0.1[a]	1.1 ± 0.05[a]
473	-0.1 ± 0.05[a]	1.8 ± 0.05[a]
498	0.3 ± 0.1[a]	1.3 ± 0.05[a]

[a] The 95% approximate individual confidence intervals.

negative, except at 498 K (Table 2), hence, increasing the inlet partial pressure of toluene, results in a decrease of the hydrogenation rate at most temperatures. This can be understood if the increase in the toluene surface coverage due to the higher toluene partial pressure results in and is overcompensated by a decrease in the H surface coverage due to competition in the chemisorption of toluene and H_2 on the metal surface. Competitive chemisorption has already been reported [7,24,27,30,32], however, most other sources only consider non-competitive chemisorption between the aromatic model component and H_2 [8,10,13,15,22,31,34]. Repulsive interactions between two chemisorbed species on neighboring sites exists [48,73–76], so that a certain kind of competition between chemisorbing H_2 and aromatic species can occur, even when different types of sites are involved. The observation of non-competitive chemisorption seems to depend on the experimental process conditions. At temperatures lower than those investigated presently the metal surface is completely saturated with aromatic species. However, between the chemisorbed aromatic species, a constant, limited number of sites exist which are available for dissociative H_2 chemisorption [36]. If, at higher temperatures, the saturation of the metal surface by aromatic species is no longer maintained, sites that were previously occupied by an aromatic species are now also available for H_2 chemisorption, explaining the competitive character of the H_2 and aromatic chemisorption at the temperatures investigated in this work. At even higher temperatures surface coverages become so small that no competition is observed.

3.2. Kinetic model assumptions and rate equation

The kinetic modeling of aromatic hydrogenation reactions based on steady state data without in situ characterization of the surface cannot make use of direct information concerning the surface intermediates. This has lead to a variety of possible kinetic models presented for the hydrogenation of aromatic model components, as discussed in Section 1. Discrimination among different kinetic models was performed by interpretation of the results of the regression of experimental data to these models. In the present work, an alternative model is developed based on insight provided by quantumchemical calculations combined with literature data on the different elementary steps.

3.2.1. Rate-determining step (RDS)

If a RDS is considered, mostly the addition of the first H atom, H_2 molecule or the simultaneous addition of the first two H atoms is selected as the RDS [10,14,22,36]. This assumption can, by analogy to gas phase conditions, be related to the breaking of the resonance stabilization of the aromatic species. However, both quantumchemical calculations and experimental results on the interaction of aromatic species with metal surfaces indicate that the presumed analogy between the hydrogenation reaction sequence in the gas phase and on the Pt-surface is not valid.

The activation energies for the addition of the first and the second H atom to a benzene ring chemisorbed on a Pt(1 1 1)-surface were obtained from quantumchemical calculations and amount to 75 and 73 kJ mol^{-1}, respectively. The similarity between those values indicates that the rate coefficient of the H atom addition to the chemisorbed benzene species is not significantly different from the rate coefficient of the H atom addition to the cyclohexadienyl species on the surface. If the addition of the first H atom to chemisorbed benzene were breaking the resonance stabilization, a higher value for the activation energy than for that of the second H atom addition would be expected.

The second argument that the analogy between the hydrogenation reaction sequence in the gas phase and on the Pt-surface species is not valid is provided in Table 3 and Fig. 4. The chemisorption enthalpies in Table 3 were calculated quantumchemically for benzene (B), H_2, and 1,4-CHD and were taken from literature for CHA and CHE [41,44]. Experimental support for the quantumchemically calculated values is available [39,41]. No significant differences were found between levels determined based on 1,3- or 1,4-CHD, hence, this component will further be addressed as CHD. The value found for H_2 represents an average of the variation in H_2 chemisorption enthalpy with the surface coverage reported by Podzolkin et al. [75]. For benzene, two possibilities were found. A reactive form, mainly occurring at high surface coverages and a non-reactive form, mainly occurring at low surface coverages. The reactive form was used to determine the enthalpy levels in Fig. 4. For CHD only one form was found. Also for CHE and CHA, only one form was reported [41,44]. In Fig. 4, the enthalpy level of gas phase CHA was set to zero. In the gas phase 'CHD + 2H_2' is at the highest enthalpy level in the hydrogenation reaction sequence. Due to the endothermicity of the dehydrogenation

Table 3
Chemisorption enthalpies of reactants, product and intermediates during the hydrogenation of benzene

Component	H_2[a]	Benzene[a]	CHD[a]	CHE[b]	CHA[b]
$-\Delta H_{chem}$ (kJ mol^{-1})	70	75[c], 117[d]	146	71	58

[a] Calculated quantumchemically.
[b] From [41,44].
[c] Reactive form.
[d] Non-reactive form.

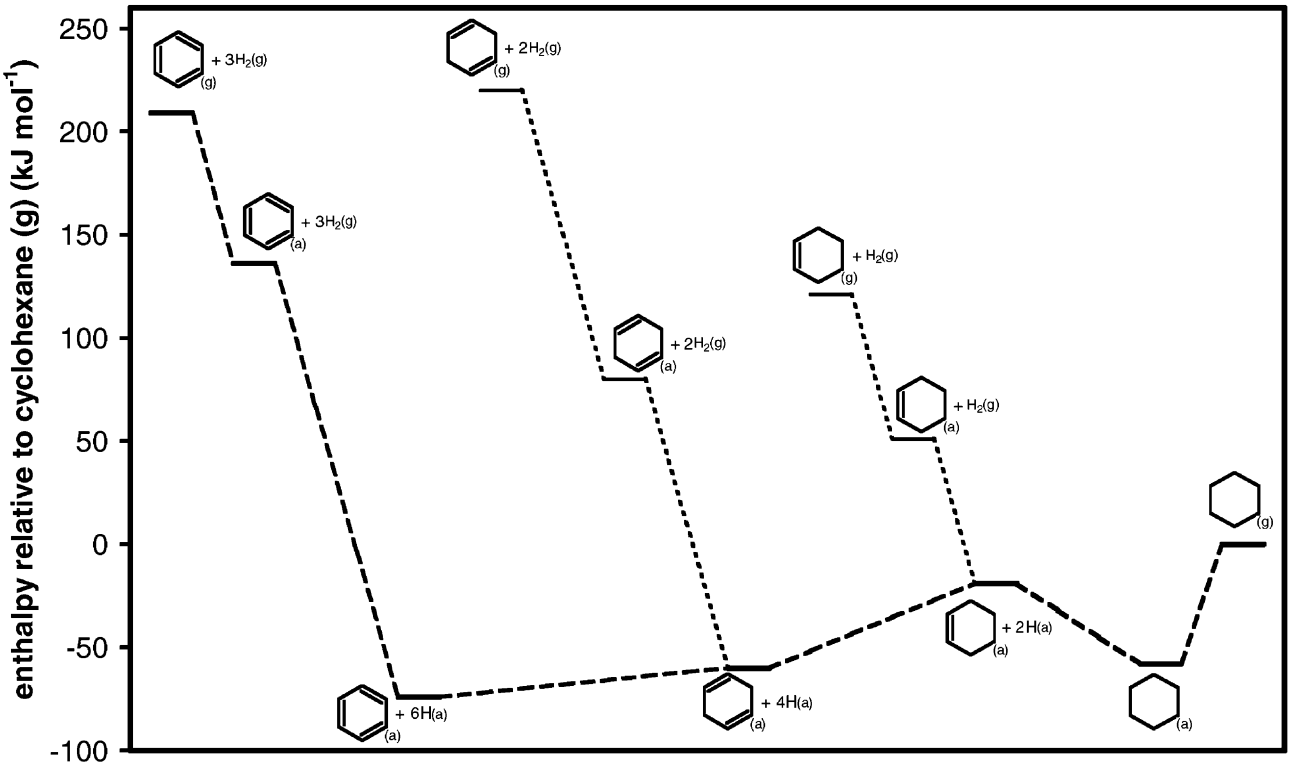

Fig. 4. Enthalpy levels for the components involved in benzene hydrogenation.

reactions 'CHA' is at a lower enthalpy level than 'CHE + H_2', which on its turn is at a lower level than 'CHD + $2H_2$'. The resonance stabilization of the aromatic ring results in a lower enthalpy level for 'B + $3H_2$' than for 'CHD + $2H_2$'. This resonance stabilization makes hydrogenation in the gas phase very difficult. Once the resonance stabilization has been broken, hydrogenation proceeds very rapidly to the totally hydrogenated product, i.e. the breaking of the resonance stabilization is the RDS in gas phase hydrogenation. On a Pt-surface, however, this picture is no longer valid. CHD chemisorbs much more strongly than benzene, so that the effect of the resonance stabilization with adsorbed benzene is at least weakened, if not entirely lost. CHE chemisorbs relatively weakly, resulting in the highest enthalpy level for 'CHE + 2H' in the hydrogenation sequence on the surface. Moreover, the enthalpy rise from 'CHD + 4H' to 'CHE + 2H' is higher than from 'B + 6H' to 'CHD + 4H'. If different activation energies for the surface reactions are assumed, then, based on an Evans–Polanyi relationship [77], a higher activation energy is expected for the third or the fourth H addition step. Hence, one of the latter steps is expected to be rate-determining, rather than the addition of the first or second H atom.

Other reaction mechanisms that have been proposed do not assume the existence of a RDS, but consider two or all hydrogen addition reactions as being not quasi-equilibrated. Van Meerten et al. [13] and Lindfors et al. [24] used the same rate coefficient for all addition steps. Chou and Vannice [15] allowed a linear distribution of standard enthalpies and entropies of activation between the first and the sixth H atom addition step and found a weak decrease and increase, respectively. The enthalpy levels during benzene hydrogenation on a Pt-surface, viz. Fig. 4, support such kind of models considering the first to the fourth H atom addition as being not quasi-equilibrated, since it shows an increasing enthalpy level (endothermicity) from benzene up to chemisorbed CHE. Further hydrogenation from CHE to CHA on the surface is exothermic and is more likely to be in quasi-equilibrium.

3.2.2. *Dehydrogenated surface species*

The minor loss of catalytic activity during hydrogenation can be attributed to the formation of H-deficient carbonaceous species on the metal surface. The coverage of active sites by surface species with an aromatic nature has already been proposed in earlier work [78,79]. In more recent communications, especially the group of Vannice considered the inclusion of a dehydrogenation reaction, concurrent to the hydrogenation reactions, involving the aromatic reactant molecule to produce H-deficient species [15,36]. Moreover, Lin and Vannice [36] postulated a single dominant H-deficient species on the surface, i.e. present in much larger amounts than the other possible H-deficient species and the aromatic species. Based on regressions of experimental data to several model equations, each with an other dominant H-deficient species, these authors found

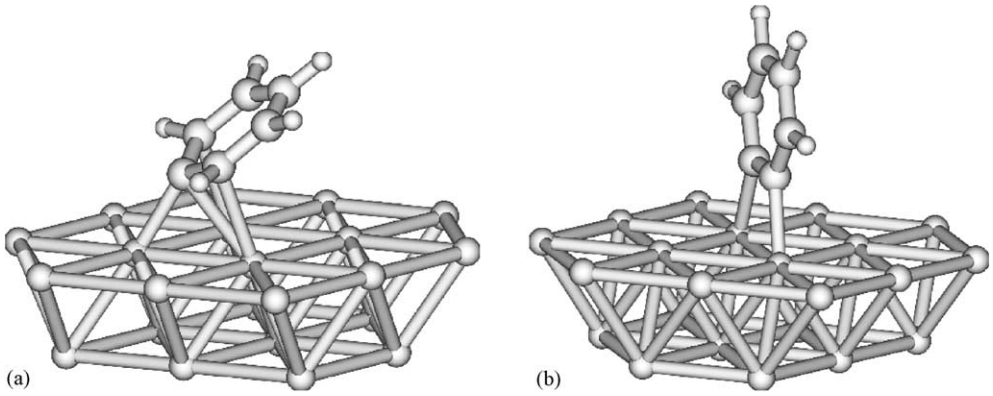

Fig. 5. Structure of adsorbed (a) phenyl and (b) benzyne from DFT BP86/double zeta calculations.

that the surface species produced by one H atom abstraction of the chemisorbed aromatic reactant was the most likely dominant surface species.

In a thermochemical study of interaction of benzene and related products with Pt-surfaces, Koel et al. [44] also considered H atom abstraction from chemisorbed benzene. Due to uncertainties about the nature of these dehydrogenated species, these authors report two possible enthalpy levels for the latter. One includes extra stabilization of the dehydrogenated species on the surfaces and has an enthalpy level only marginally lower than that of chemisorbed benzene, while the other is more than 100 kJ mol^{-1} higher in enthalpy level [44]. Quantumchemical calculations have been performed to obtain insight in the benzene dehydrogenation reactions. Different pathways were studied. The most stable phenyl and benzyne intermediates are shown in Fig. 5. The binding of the ring π-system to the Pt-surface is broken. The reaction enthalpy for dehydrogenation depends on the hydrogen adsorption energy, which is strongly coverage dependent [75]. The endothermicity of the benzene dehydrogenation to phenyl is between 76 and 102 kJ mol^{-1} and to benzyne between 13 and 66 kJ mol^{-1}. Therefore, our ab initio calculations provide evidence for the higher energetic species of the two reported by Koel et al. [44]. Hence, if an equilibrium between the chemisorbed aromatic reactant and its dehydrogenated counterpart is established on the metal surface, it seems unlikely that the H-deficient species would be the most abundant surface intermediate. Also kinetically the dehydrogenation of benzene is limited, since the activation energy has to be higher than 76–102 kJ mol^{-1}.

3.2.3. Reactant chemisorption, product desorption and H_2 spillover

As discussed in Section 3.1, the observed toluene partial pressure effect on the hydrogenation rate is believed to originate from competitive chemisorption of the aromatic reactant and H_2 on the metal surface. It is, therefore, necessary to include competitive chemisorption in the kinetic model. H_2 and toluene chemisorption were assumed to be in quasi-equilibrium, in agreement with other literature models [13,15,22,24,36]. The desorption of methylcyclohexane is assumed to be fast and irreversible since its surface coverage can be assumed to be negligible in accordance with Van Meerten et al. [13].

If hydrogenation reactions are performed on typical hydrogenation metals supported by an acidic carrier, such as an alumina-silicate or a zeolite, a hydrogenation rate enhancement is observed compared to hydrogenation rates on unsupported metals or metals supported by an essentially non-acidic support, such as silica or alumina [15,19,22,23,25,36–38]. Two mechanisms have been proposed to explain this increase in hydrogenation rate. The first mechanism considers metal-support interactions, which modify the electronic state of the metal cluster on the support and make it more active for hydrogenation reactions [35]. The second one, called H_2 spillover, has been developed more recently and has received by now most attention in the literature [15,19,22,23,25,36–38]. Following this mechanism aromatic reactant molecules that are adsorbed on acidic sites 'close' to a metal cluster can be hydrogenated by hydrogen that is 'spilled over' from that metal cluster.

The Pt on the ZSM-22 used in this work is deposited on the external surface of the zeolite, i.e. in the intercrystalline pores, remote from the acid sites. Hence, no rate enhancement due to H_2 spillover is expected to occur.

3.2.4. Rate equation

The assumptions about the reaction mechanism based on which the rate equation for toluene hydrogenation was developed are summarized in Table 4. These assumptions lead to the following sequence of elementary steps

$$H_2(g) + 2^* \leftrightarrow 2H^* \quad (K_{H_2}) \tag{6}$$

$$A(g) + * \leftrightarrow A^* \quad (K_A) \tag{7}$$

$$A^* + H^* \overset{k_1}{\rightleftarrows} AH^* + * \quad (K_1) \tag{8}$$

$$AH^* + H^* \overset{k_2}{\rightleftarrows} AH_2^* + * \quad (K_2) \tag{9}$$

Table 4
Assumptions for the general model analogous to Horiuti Polanyi mechanism [80]

1	No RDS exists: the first four H atom additions steps are not quasi-equilibrated, while the fifth and the sixth H atom addition are
2	H_2 (dissociative chemisorption) and aromatic reactant both chemisorb on identical sites (competitive chemisorption)
3	(a) H_2 and aromatic reactant chemisorption are quasi-equilibrated (b) Desorption of the hydrogenated product is fast and irreversible
4	No dehydrogenated surface species are considered

$$AH_2^* + H^* \overset{k_3}{\rightleftarrows} AH_3^* + * \quad (K_3) \tag{10}$$

$$AH_3^* + H^* \overset{k_4}{\rightleftarrows} AH_4^* + * \quad (K_4) \tag{11}$$

$$AH_4^* + H^* \leftrightarrows AH_5^* + * \quad (K_5) \tag{12}$$

$$AH_5^* + H^* \leftrightarrows AH_6^* + * \quad (K_6) \tag{13}$$

$$AH_6^* \rightarrow AH_6(g) + * \tag{14}$$

For finite values of K_5 and K_6, assumption 3(b) causes the quasi-equilibrium of reactions (12) and (13) to shift to the right, so that also the AH_4^* and AH_5^* coverage are negligible. Hence, the net rate of AH_6(g)-production can be written as

$$R_{AH_6(g)} = C_t k_4 \theta_{AH_3^*} \theta_{H^*} \tag{15}$$

Applying the pseudo steady state approximation for the species AH^*, AH_2^*, and AH_3^*, the following mass balances can be written for AH^* and AH_2^*

$$k_i \theta_{AH_{i-1}^*} \theta_{H^*} + \frac{k_{i+1}}{K_{i+1}} \theta_{AH_{i+1}^*} \theta_* - k_{i+1} \theta_{AH_i^*} \theta_{H^*} - \frac{k_i}{K_i} \theta_{AH_i^*} \theta_* = 0 \quad (i = 1, 2) \tag{16}$$

and for AH_3^*:

$$0 = k_3 \theta_{AH_2^*} \theta_{H^*} - k_4 \theta_{AH_3^*} \theta_{H^*} - \frac{k_3}{K_3} \theta_{AH_3^*} \theta_* \tag{17}$$

via expressions for the chemisorption equilibria, surface coverages are related to gas phase partial pressures:

$$\theta_{A^*} = \theta_* K_A p_A \tag{18}$$

$$\theta_{H_2^*} = \theta_* \sqrt{K_{H_2} p_{H_2}} \tag{19}$$

a site balance:

$$\theta_* + \theta_{H^*} + \theta_{A^*} + \theta_{AH^*} + \theta_{AH_2^*} + \theta_{AH_3^*} = 1 \tag{20}$$

completes the set of algebraic equations. Eqs. (4) and (15)–(20) describe fully the hydrogenation kinetics.

4. Modeling results and discussion

4.1. General model analogous to the Horiuti Polanyi mechanism

In this stage of model development, nine different coefficients are involved. These are four forward rate coefficients (k_1–k_4), three surface reaction equilibrium coefficients (K_1–K_3), and two chemisorption coefficients (K_A and K_{H_2}). Hence, for application of the model under non-isothermal conditions 18 parameters have to be determined. This is a large number to be obtained by regression of experimental data since there is only one independent response. Therefore, a reduction of the number of parameters to be obtained by regression is performed by calculation of preexponential factors and by the introduction of extra model assumptions [80].

The preexponential factors of the four forward reaction rate coefficients can be calculated based on transition state theory [73,74,76,77]. Regarding the uncertainty about the surface mobility of the intermediates, the same value is used for the preexponential factors of the surface reaction rate and equilibrium coefficients. Depending on the assumed surface mobility of the chemisorbed toluene species, a value in the range 10^{-10} to $10^{-13}\,Pa^{-1}$ is calculated for the preexponential factor of the toluene chemisorption equilibrium coefficient for a mobile and a immobile species, respectively. Similar considerations lead to a range from 10^{-8} to $10^{-13}\,Pa^{-1}$ for the preexponential factor of the H_2 chemisorption equilibrium coefficient. This range is more extended due to the dissociative character of H_2 chemisorption. The preexponential factor for the surface reaction rate coefficient is calculated to be in the range 10^8 to $10^{13}\,s^{-1}$ if all species, i.e. reactants and transition state, are mobile or immobile, respectively. However, this range can be even more extended if species with different surface mobilities are involved. Via analogous considerations the value for the preexponential factor of reverse surface reaction rate coefficients amounts to approximately $10^{13}\,s^{-1}$. One single value is reported since the reverse reaction is monomolecular and since the same mobility is assumed for the reactant and the transition state. If the transition state would have a higher mobility than the reactant, a higher value would be obtained. By division of the preexponential factor of the forward and the reverse surface reaction rate coefficient, a range for the preexponential factor of the surface reaction equilibrium coefficients from 1 to 10^{-5} is obtained. Nine parameters are remaining, i.e. four activation energies, three surface reaction enthalpies and two chemisorption enthalpies. Further reduction of the number of parameters could be performed via an Evans–Polanyi correlation [77] relating the activation energies with the reaction enthalpies, however, this would only reduce the number of parameters from nine to eight and is therefore discarded.

Two possibilities are considered for further reduction of the number of parameters. The preexponential factors of the surface reaction rate coefficients were set equal to each other,

i.e. $k^0_{surf} = k^0_i$ for $i = 1$–4, regarding the assumed similarity between the different H atom addition steps. Based on this assumption it is straightforward to assume that also the activation energies of the surface reactions can be set equal to each other. Also the equality of the surface reaction enthalpies can be assumed, leading to a kinetic model with equal surface reaction rate and equilibrium coefficients [13,24]. In such a model, no RDS is assumed. On the other hand, based on the enthalpy levels shown in Fig. 4 and the discussion in Section 3.2.1, the addition of the third or the fourth H atom could be expected to be rate-determining because of the higher activation energies associated with these steps. Moreover, CHE and CHA dehydrogenation studies provided evidence for a stable π-allylic cyclohexenyl (cC_6H_9) intermediate on the surface [40,43,45]. This could be related to the occurrence of a RDS corresponding to the third or fourth H atom addition step, since in these steps such a species is respectively produced and consumed.

4.2. Model without rate-determining step and with equal surface reaction rate coefficients

The rate equation corresponding to the kinetic model with equal surface reaction rate coefficients is obtained by elimination of the surface coverages from the set of equations describing the hydrogenation kinetics, i.e. Eqs. (4) and (15)–(20). The surface coverage of *A*H, AH_2, and AH_3 can be expressed in terms of the chemisorbed toluene coverage A^* (Eqs. (16) and (17)) as

$$\theta_{AH_3^*} = \frac{B\theta_{AH_2^*}}{B+1} = \frac{B^2\theta_{AH^*}}{B^2+B+1} = \frac{B^3\theta_{A^*}}{B^3+B^2+B+1} \quad (21)$$

in which $B = K_{surf}\theta_{H^*}/\theta_* = K_{surf}\sqrt{K_{H_2}p_{H_2}}$. The toluene and H atom surface coverage can be related to each other by division of the chemisorption equilibrium expressions:

$$\theta_{H^*} = \frac{\sqrt{K_{H_2}p_{H_2}}}{K_A p_A}\theta_{A^*} \quad (22)$$

Combination of Eqs. (18) and (20)–(22) leads to the following expression for the toluene surface coverage:

$$\theta_{A^*} = \frac{K_A p_A(B^3+B^2+B+1)}{(B^3+B^2+B+1)(1+\sqrt{K_{H_2}p_{H_2}}) + K_A p_A(4B^3+3B^2+2B+1)} \quad (23)$$

An analogous equation can be derived for θ_{H^*}, which can then be substituted into Eq. (15) resulting in the rate equation:

$$R_{AH_6(g)} = C_t k_{surf}\frac{B^3 K_A p_A\sqrt{K_{H_2}p_{H_2}}(B^3+B^2+B+1)}{((B^3+B^2+B+1)(1+\sqrt{K_{H_2}p_{H_2}}) + K_A p_A(4B^3+3B^2+2B+1))^2} \quad (24)$$

Table 5
Values for the preexponential factors calculated based on transition state theory [73,74,77]

k^0_{surf} (s^{-1})	K^0_{surf}	K^0_A (Pa^{-1})	$K^0_{H_2}$ (Pa^{-1})
10^{15}	10^{-2}	10^{-12}	10^{-10}

This rate equation is similar to the one proposed by Van Meerten et al. [13], however, in this case competitive chemisorption of H_2 and the aromatic reactant is considered and only the first four H atom addition steps are assumed not being quasi-equilibrated, instead of all H atom additions.

In the model with equal surface reaction rate coefficients for the H atom addition steps, four parameters or parameter groups are to be obtained by regression: one surface reaction enthalpy (ΔH_{surf}), two chemisorption enthalpies (ΔH_A and ΔH_{H_2}) and one composite activation energy ($E^{comp}_{act,surf} = E_{act,surf} + \Delta H_A + 0.5\Delta H_{H_2}$). Preliminary regressions resulted in an especially low *t*-value for the enthalpies contained in the factor *B*, i.e. $\Delta H_{surf} + 0.5\Delta H_{H_2}$. The insensitivity to the value of this sum of enthalpies indicates that it is close to zero and, hence, that $\Delta H_{surf} \approx -0.5\Delta H_{H_2}$. The factor *B* has a weak temperature dependence, which is even too weak to be significantly estimated. Several sets of values for the preexponential factors were tested, each corresponding with different assumptions concerning the surface mobility of the H atoms, the hydrocarbon species and the transition states. The optimal set, viz. Table 5, corresponded with mobile H atoms on the catalyst surface, i.e. two translational degrees of freedom, while the reactant and product hydrocarbon surface species were found to be rather immobile, i.e. no translational degrees of freedom, but one rotational degree of freedom. The transition states were found to have a higher surface mobility than the other hydrocarbon species. This can be related to the conservation of one of the H atom translational degrees of freedom during its addition the hydrocarbon species. A regression with these preexponential factors from Table 5 and with an average surface reaction equilibrium coefficient for all temperatures lead to the estimates and corresponding 95% approximate individual confidence intervals for the remaining parameters reported in Table 6. Although the H_2 chemisorption enthalpy was estimated significantly, the corresponding *t*-value was almost a factor 10 lower than the *t*-value of the toluene chemisorption enthalpy. However, this is logical if the H atom surface coverage is low compared to the toluene surface coverage, so that the model is less sensitive to the H_2 chemisorption parameters. The fractional surface coverages at typical reaction conditions, i.e. $T = 450$ K, $p_{H_{2,0}} = 100$ kPa and $p_{tol,0} = 20$ kPa, amount to 0.19 for H_2 and to 0.59 for toluene and support the above. The fraction of the surface occupied by other hydrocarbon species is small, i.e. <0.01. Binary correlation coefficients between the parameters are lower than 0.95, except between the composite activation energy and the H_2 chemisorption enthalpy, where a value of 0.97 is found. This correlation is however in

Table 6
Parameter estimates obtained by regression of the three kinetic models used, Eqs. (4) and (24), respectively Eqs. (4) and (28) with $i = 3$, 4 and with the preexponential factors from Table 5

	$E^{comp}_{act,surf}$ (kJ mol^{-1})	ΔH_{H_2} (kJ mol^{-1})	ΔH_A (kJ mol^{-1})
Model with equal surface reaction rate coefficients	−53[b] ± 5[a]	−42 ± 12[a]	−70 ± 2[a]
Model with the third H atom addition as the RDS	−51[c] ± 1[a]	N.S.[e]	−68 ± 1[a]
Model with the fourth H atom addition as the RDS	−59[d] ± 7[a]	−42 ± 12[a]	−70 ± 2[a]

[a] The 95% approximate individual confidence intervals.
[b] $E^{comp}_{act,surf} = E_{act,surf} + \Delta H_A + 0.5\Delta H_{H_2}$.
[c] $E^{comp}_{act,surf} = E_{act} + \Delta H_A + 1.5\Delta H_{H_2} + \Delta H_1 + \Delta H_2$.
[d] $E^{comp}_{act,surf} = E_{act} + \Delta H_A + 2\Delta H_{H_2} + \Delta H_1 + \Delta H_2 + \Delta H_3$.
[e] Not significant.

agreement with the lower surface coverage by H_2. The value of the denominator is relatively insensitive to variations in the H_2 chemisorption enthalpy, while in the numerator such variations strongly affect the value of B, viz. Eq. (21), and are compensated by variations in the composite activation energy. The corresponding F-value for the significance of the regression amounts to 10^4. The parity diagram in Fig. 6 shows the agreement of the calculated with the experimental methylcyclohexane outlet flow rates. The toluene chemisorption enthalpy, −70 kJ mol^{-1}, is a little less exothermic than the benzene chemisorption enthalpy, −75 kJ mol^{-1} corresponding with the reactive form calculated quantumchemically, viz. Table 3. The weaker chemisorption of toluene than of benzene explains its lower hydrogenation rate [19,23]. The value for the H_2 chemisorption enthalpy is estimated less negative, i.e. −42 kJ mol^{-1}, than quantumchemically calculated, −70 kJ mol^{-1}. However, the 95% approximate individual confidence interval is rather large and intersects the range of H_2 chemisorption enthalpies reported by Podzolkin et al. [75]. From the value of the composite activation energy, the real activation energy is calculated and amounts to 38 kJ mol^{-1}. This is lower than what was calculated quantumchemically, however, the weak exothermicity estimated for H_2 chemisorption partly accounts for this effect. Using the value reported in Table 3, a value closer to the quantumchemically calculated values is obtained, i.e. 52 kJ mol.

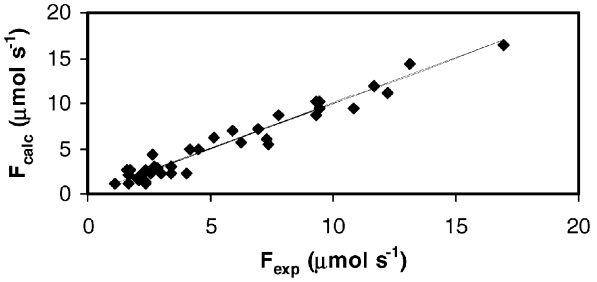

Fig. 6. Parity diagram for the methylcyclohexane outlet flow rate; line: experimental, dots: calculated based on the kinetic model with equal surface reaction rate coefficients, Eqs. (4) and (24) with the preexponential factors from Table 5 and the composite activation energy and chemisorption enthalpies from Table 6.

4.3. Model with a rate-determining step (RDS)

The other possibility mentioned in Section 4.1 was the introduction of the third or the fourth H atom addition as the RDS, related to the occurrence of a cyclohexenyl species (cC_6H_9) on the surface. Derivation of the rate equation starts from

$$R_{AH_6(g)} = C_t k_i \theta_{AH^*_{i-1}} \theta_{H^*} \quad (i = 3, 4) \tag{25}$$

where i represents the number of the rate-determining H atom addition step. The quasi-equilibrium for the other H atom additions allows us to relate $\theta_{AH^*_{i-1}}$ to θ_{A^*} as

$$\theta_{AH^*_{i-1}} = \left(\prod_{j=1}^{i} K_j\right) \frac{\theta_{A^*} \theta^{i-1}_{H^*}}{\theta^{i-1}_*} \quad (i = 3, 4) \tag{26}$$

The surface coverages are obtained from the corresponding partial pressures via Eqs. (18) and (19). Hydrocarbon species other than the aromatic reactant are not considered which is justified by the endothermicity of the first four H atom addition steps (Fig. 4). Therefore, the site balance, Eq. (20) is reduced to:

$$1 = \theta_* + \theta_{A^*} + \theta_{H^*} \tag{27}$$

Combination of Eqs. (25)–(27) leads to the following rate equation:

$$R_{AH_6(g)} = \frac{C_t k_i \left(\prod_{j=1}^{i} K_j\right) K_A K^{i/2}_{H_2} p_A p^{i/2}_{H_2}}{(1 + K_A p_A + \sqrt{K_{H_2} p_{H_2}})^2} \quad (i = 3, 4) \tag{28}$$

The rate parameters were estimated by a non-isothermal regression of this rate equation for $i = 3$, 4 to all experimental data. Initial regressions for $i = 3$ showed that the model calculations were insensitive to the chemisorption of H_2, such that the H_2 chemisorption term was removed from the denominator. Similar conclusions on the surface mobilities of the species were drawn, so that the same values as in Table 5 were used. The remaining parameters are the composite activation energy ($E^{comp}_a = E_a + \Delta H_A + 1.5\Delta H_{H_2} + \Delta H_1 + \Delta H_2$) and the toluene chemisorption enthalpy (ΔH_A). Their estimates and

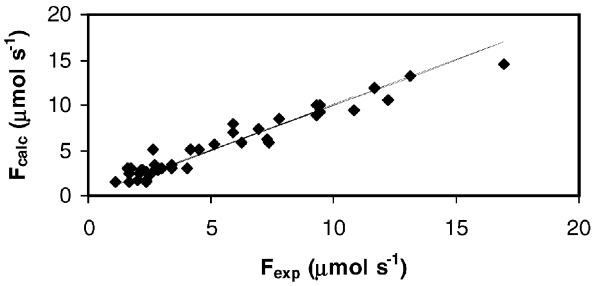

Fig. 7. Parity diagram for the methylcyclohexane outlet flow rate; line: experimental, dots: calculated based on the kinetic model with the third H addition as the RDS, Eqs. (4) and (28) with $i = 3$ and with the preexponential factors from Table 5 and the composite activation energy and chemisorption enthalpies from Table 6.

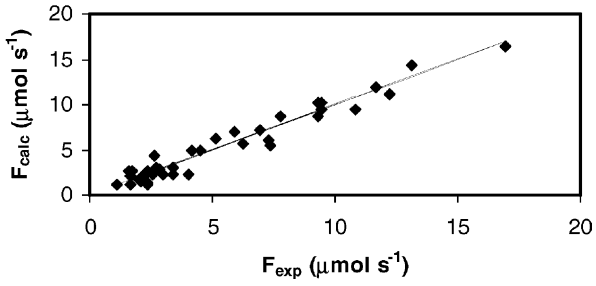

Fig. 8. Parity diagram for the methylcyclohexane outlet flow rate; line: experimental, dots: calculated based on the kinetic model with the fourth H addition as the RDS, Eqs. (4) and (28) with $i = 4$ and with the preexponential factors from Table 5 and the composite activation energy and chemisorption enthalpies from Table 6.

corresponding 95% approximate individual confidence intervals are reported in Table 6. An F-value of 5×10^2 was obtained. The agreement between the calculated and experimental methylcyclohexane outlet flow rate is shown in Fig. 7. The agreement is good, but somewhat inferior to the one obtained with the model with equal surface reaction rate coefficients, which is also reflected in the respective F-values. The value obtained for toluene chemisorption enthalpy, $-68\,\mathrm{kJ\,mol^{-1}}$, is in agreement with that obtained with the model with equal surface reaction rate coefficients. Using a H_2 chemisorption enthalpy of 70 and $13\,\mathrm{kJ\,mol^{-1}}$ endothermicity between A^* and AH_2^* (Fig. 4), a value of $109\,\mathrm{kJ\,mol^{-1}}$ is obtained for the real activation energy starting from the composite activation energy. Using the weakest H_2 chemisorption enthalpy reported by Podzolkin et al. [75], i.e. $50\,\mathrm{kJ\,mol^{-1}}$, the value for the real activation energy amounts to $80\,\mathrm{kJ\,mol^{-1}}$, which is somewhat higher than the values calculated quantumchemically and on the high end of the range reported in the literature [34].

Taking the fourth H atom addition as the RDS, all parameters, i.e. the composite activation energy ($E_a^{comp} = E_a + \Delta H_A + 2\Delta H_{H_2} + \Delta H_1 + \Delta H_2 + \Delta H_3$) and the H_2 and toluene chemisorption enthalpies, could be estimated significantly. The conclusions concerning the surface mobilities of the species were analogous to those made above, hence the same values as in Table 5 were used. The values and their corresponding 95% approximate individual confidence intervals are reported in Table 6. An F-value of 10^4 was obtained. Fig. 8 shows the agreement between calculated and experimental methylcyclohexane outlet flow rates. H_2 chemisorption is estimated to be weaker than expected, analogous to the results obtained with the model with equal surface reaction rate coefficients. Using a $30\,\mathrm{kJ\,mol^{-1}}$ endothermicity between A^* and AH_3^* (Fig. 4), a value of $65\,\mathrm{kJ\,mol^{-1}}$ is obtained for the real activation energy starting from the composite activation energy. However, if the relationship $\Delta H_{surf} \approx -0.5\Delta H_{H_2}$ obtained based on the model with equal surface reaction rate coefficients is used, then with an endothermicity of $60\,\mathrm{kJ\,mol^{-1}}$ a real activation energy of $35\,\mathrm{kJ\,mol^{-1}}$ is found. Using a value for the H_2 chemisorption enthalpy of $-70\,\mathrm{kJ\,mol^{-1}}$ and the same relation as above, the value for the real activation energy amounts to $46\,\mathrm{kJ\,mol^{-1}}$.

4.4. Model selection

From the three models tested in this work, the model with equal surface reaction rate coefficients and the model with the fourth H atom addition as the RDS have the highest F-values for significance of the regression. In those two models the chemisorption enthalpies for toluene and H_2 could be significantly estimated simultaneously. Also the parity diagrams for those two models were very similar. This similar behavior indicates that the model with the fourth H atom addition as the RDS is a limit of the more general model with equal surface reaction rate coefficients. In this limiting case, the surface coverage of the partially hydrogenated surface species decreases as the number of added H atoms increases. This effect appears from Eq. (21) for values of B which are sufficiently lower than one, but not zero. With sufficiently large differences in surface coverage, also the differences in the forward reaction rates will be large because of the equal surface reaction rate coefficients used. Hence, the forward reaction of the surface species with the lowest surface coverage becomes rate-determining. In that limiting case, the model with equal surface reaction rate coefficients (24) becomes mathematically equal to the model with the fourth H atom addition as the RDS, Eq. (28) with $i = 4$. Because of this more general character of the model with equal surface reaction rate coefficients, this model is selected. A similar conclusion was drawn by Van Meerten et al. [13].

5. Conclusions

Careful consideration of various aspects encountered in the kinetic modeling of aromatic component hydrogenation has yielded important new insights in the hydrogenation reaction mechanism. It was shown that the rate-determining effect of the resonance stabilization in the gas phase is lost upon chemisorption on the catalyst surface. Although a

certain loss of catalytic activity occurred, the presence of dehydrogenated species as most abundant surface intermediate in equilibrium with the aromatic reactant can be rejected. An identical type of sites was assumed for H_2 and toluene. A thermochemical analysis of the hydrogenation of benzene on a Pt-surface suggested the quasi-equilibration of the last two H atom addition steps.

A model with equal surface reaction rate coefficients for the first four H atom addition steps and assuming quasi-equilibrium for the fifth and the sixth H atom addition was selected as the best model, based on its flexibility. According to this model, the hydrocarbon species are relatively immobile on the catalyst surface, while the H atoms have a higher mobility. The surface coverage by H atoms is non-negligible, but is lower than the surface coverage by aromatic reactant molecules. The activation energy and chemisorption enthalpies estimated with this model are close to values calculated quantumchemically and reported in literature.

Acknowledgements

This research was carried out in the framework of “Inter University Attraction Poles”, funded by the Belgian Government and the DWTC Office. The 0.5 wt.% Pt/ZSM-22 catalyst was provided by J.A. Martens and P.A. Jacobs (Katholieke Universiteit Leuven).

References

[1] B.H. Cooper, B.B.L. Donnis, Appl. Catal. A: Gen. 137 (1996) 203–223.
[2] L. Allen, World Fuels Meeting Fall, 1998, http://www.criterioncatalysts.com/pdfs/WrldFls98.pdf.
[3] G.G. Martens, G.F. Froment, Stud. Surf. Sci. Catal. 122 (1999) 333–340.
[4] G.G. Martens, G.B. Marin, P.A. Jacobs, J.A. Martens, G.V. Baron, J. Catal. 195 (2000) 253–267.
[5] G.G. Martens, J.W. Thybaut, G.B. Marin, Ind. Eng. Chem. Res. 40 (2001) 1832–1844.
[6] L.N. Canjar, F.S. Manning, J. Appl. Chem. 12 (1962) 73–75.
[7] J.E. Germain, R. Maurel, Y. Bourgeois, R. Sinn, J. Chim. Phys. 60 (1963) 2319–2330.
[8] Y.S. Snagovskii, G.Y. Lyubarski, G.M. Ostrovskii, Kinet. Katal. 2 (1966) 258–265.
[9] N.E. Zlotina, S.L. Kiperman, Kinet. Katal. 6 (1967) 1335–1341.
[10] F. Jiracek, J. Pasek, J. Horak, Coll. Czech. Chem. Commun. 33 (1968) 3266–3279.
[11] K.P. Roethe, A. Roete, B. Rosahl, D. Gelbin, Chem. Ing. Tech. 42 (1970) 805–811.
[12] J.P.G. Kehoe, J.B. Butt, J. Appl. Chem. Biotechnol. 22 (1972) 23–30.
[13] R.Z.C. Van Meerten, T.F.M. De Graaf, J.W.E. Coenen, J. Catal. 46 (1977) 1–12;
R.Z.C. Van Meerten, J.W.E. Coenen, J. Catal. 46 (1977) 13–24.
[14] C. Mirodatos, J.A. Dalmon, G.A. Martin, J. Catal. 105 (1987) 405–415.
[15] P. Chou, M.A. Vannice, J. Catal. 107 (1987) 129–139;
P. Chou, M.A. Vannice, J. Catal. 107 (1987) 140–153.
[16] B. Coughlan, M.A. Keane, Zeolites 11 (1991) 12–17.
[17] N.M. Ostrovskii, A. Parmaliana, F. Frusteri, L.P. Maslova, N. Giordano, Kinet. Catal. 32 (1991) 67–73.
[18] P. Reyes, I. Concha, M.E. Konig, E. Delgado, Bol. Soc. Chil. Quim. 36 (1991) 147–152.
[19] S.D. Lin, M.A. Vannice, J. Catal. 143 (1993) 539–553.
[20] S.S. Au, J.S. Dranoff, J.B. Butt, Chem. Eng. Sci. 50 (1995) 3801–3812.
[21] F. Dobert, J. Gaube, Ind. Eng. Chem. Res. 35 (1996) 1824–1833.
[22] M.V. Rahaman, M.A. Vannice, J. Catal. 127 (1991) 251–266;
M.V. Rahaman, M.A. Vannice, J. Catal. 127 (1991) 267–275.
[23] S.D. Lin, M.A. Vannice, J. Catal. 143 (1993) 554–562.
[24] L.P. Lindfors, T. Salmi, S. Smeds, Chem. Eng. Sci. 48 (1993) 3813–3828.
[25] J. Chupin, N.S. Gnep, S. Lacombe, M. Guisnet, Appl. Catal. A: Gen. 206 (2001) 43–56.
[26] J.L. Rousset, L. Stievano, F.J. Cadete Santos Aires, C. Geantet, A.J. Renouprez, M. Pellarin, J. Catal. 197 (2001) 335–343.
[27] S. Smeds, D. Murzin, T. Salmi, Appl. Catal. A: Gen. 125 (1995) 271–291.
[28] T.-C. Huang, B.-C. Kang, Ind. Eng. Chem. Res. 34 (1995) 2955–2963;
T.-C. Huang, B.-C. Kang, Ind. Eng. Chem. Res. 34 (1995) 1140–1148.
[29] S. Smeds, D. Murzin, T. Salmi, Appl. Catal. A: Gen. 141 (1996) 207–228.
[30] S. Smeds, T. Salmi, D. Murzin, Appl. Catal. A: Gen. 145 (1996) 253–265.
[31] M.A. Keane, J. Catal. 166 (1997) 347–355.
[32] S. Smeds, D. Murzin, T. Salmi, Appl. Catal. A: Gen. 150 (1997) 115–129.
[33] J. Quartaro, S. Mignard, S. Kasztelan, Catal. Lett. 61 (1999) 167–172.
[34] M.A. Keane, P.M. Patterson, Ind. Eng. Chem. Res. 38 (1999) 1295–1305.
[35] F. Figueras, R. Gomez, M. Primet, Adv. Chem. Ser. 121 (1973) 480–488.
[36] S.D. Lin, M.A. Vannice, J. Catal. 143 (1993) 563–572.
[37] J. Wang, L. Huang, Q. Li, Appl. Catal. A: Gen. 175 (1998) 191–199.
[38] J. Wang, Q. Li, J. Yao, Appl. Catal. A: Gen. 184 (1999) 181–188.
[39] M.B. Hugenschmidt, A.L. Diaz, C.T. Campbell, J. Phys. Chem. 96 (1992) 5974–5978.
[40] D.P. Land, W. Erley, H. Ibach, Surf. Sci. 289 (1993) 237–246.
[41] C. Xu, Y.-L. Tsai, B.E. Koel, J. Phys. Chem. 98 (1994) 585–593;
C. Xu, B.E. Koel, M.A. Newton, N.A. Frei, C.T. Campbell, J. Phys. Chem. 99 (45) (1994) 16670–16675.
[42] S. Haq, D.A. King, J. Phys. Chem. 100 (1996) 16957–16965.
[43] J.W. Peck, B.E. Koel, J. Am. Chem. Soc. 118 (1996) 2708–2717.
[44] B.E. Koel, D.A. Blank, E.A. Carter, J. Mol. Catal. A: Chem. 131 (1998) 39–53.
[45] X. Su, K. Kung, J. Lahtinen, R.Y. Shen, G.A. Somorjai, Catal. Lett. 54 (1998) 9–15.
[46] W. Ranke, W. Weiss, Surf. Sci. 465 (2000) 317–330.
[47] P. Sautet, M.-L. Bocquet, Phys. Rev. B 53 (1996) 4910–4925.
[48] E.W. Hansen, M. Neurock, J. Catal. 196 (2000) 241–252.
[49] P.A. Jacobs, J.A. Martens, Stud. Surf. Sci. Catal. 33 (1987) 24.
[50] J.A. Martens, R. Parton, L. Uytterhoeven, P.A. Jacobs, G.F. Froment, Appl. Catal. 76 (1991) 95–116.
[51] R. Parton, L. Uytterhoeven, J.A. Martens, P.A. Jacobs, Appl. Catal. 76 (1991) 131–142.
[52] J.A. Martens, G. Vanbutsele, P.A. Jacobs, J. Denayer, R. Ocakoglu, G. Baron, J.A. Muñoz Arroyo, J. Thybaut, G.B. Marin, Catal. Today 65 (2001) 111–116.
[53] A.N.R. Bos, L. Lefferts, G.B. Marin, M.H.G.M. Steijns, Appl. Catal. A: Gen. 160 (1997) 185–190.
[54] R.J. Berger, E.H. Stitt, G.B. Marin, F. Kapteijn, J.A. Moulijn, CATTECH 5 (2001) 30–60.
[55] J.M. Berty, Chem. Eng. Progr. 70 (1974) 78–84.

[56] M. Steijns, G. Froment, P. Jacobs, J. Uytterhoeven, J. Weitkamp, Ind. Eng. Chem. Prod. Res. Dev. 20 (1981) 660–668.
[57] J.L. Dierickx, P.M. Plehiers, G.F. Froment, J. Chromat. 362 (1986) 155–174.
[58] W.A. Dietz, J. G.C., February (1967) 68–71.
[59] H.H. Rosenbrock, Comput. J. 3 (1960) 175–184.
[60] D.W. Marquardt, Ind. Appl. Math. 11 (1963) 431–439.
[61] Netlib, http://www.netlib.org.
[62] P.T. Boggs, R.H. Byrd, J.E. Rogers, R.B. Schnabel, NISTIR, 92–4834 (1992).
[63] R.G. Parr, W. Yang, Density-Functional Theory of Atoms and Molecules, Oxford University Press, New York, 1989.
[64] G. Te Velde, F.M. Bickelhaupt, E.J. Baerends, C. Fonseca Guerra, S.J.A. Van Gisbergen, J.G. Snijders, T. Ziegler, J. Comp. Chem. 22 (2001) 931–967.
[65] A.D. Becke, Phys. Rev. A 38 (1988) 3098–3100.
[66] J.P. Perdew, Phys. Rev. B 33 (1986) 8822–8824.
[67] S.H. Vosko, L. Wilk, M. Nusair, Can. J. Phys. 58 (1980) 1200–1211.
[68] E. van Lenthe, E.J. Baerends, J.G. Snijders, Chem. Phys. 99 (1993) 4597–4610.
[69] G.A. Somorjai, Introduction to Surface Chemistry and Catalysis, Wiley, New York, 1994.
[70] M. Saeys, M.-F. Reyniers, G.B. Marin, M. Neurock, J. Phys. Chem. A, submitted for publication.
[71] M. Saeys, M.-F. Reyniers, G.B. Marin, M. Neurock, Surf. Sci., submitted for publication.
[72] M. Neurock, R.A. van Santen, J. Phys. Chem. B 104 (2000) 11127.
[73] V.P. Zhdanov, Elementary Physicochemical Processes on Solid Surfaces, Plenum Press, New York, 1991.
[74] R.A. van Santen, J.W. Niemantsverdriet, Chemical Kinetics and Catalysis, Plenum Press, New York, 1995.
[75] S.G. Podkolzin, R.M. Watwe, Q. Yan, J.J. de Pablo, J.A. Dumesic, J. Phys. Chem. B 105 (2001) 8550–8562.
[76] M. Boudart, G. Djéga-Mariadassou, Cinétique des Réactions en Catalyse Hétérogène, Masson, Paris, 1982.
[77] J.A. Dumesic, D.F. Rudd, L.M. Aparicio, J.E. Rekoske, A.A. Treviño, The Microkinetics of Heterogeneous Catalysis, American Chemical Society, Washington, DC, 1993.
[78] J. Völter, M. Hermann, K. Heise, J. Catal. 12 (1968) 307.
[79] K.H.V. Prasad, K.B.S. Prasad, M.M. Mallikarjunan, R. Vaidyeswaran, J. Catal. 84 (1983) 65.
[80] J. Horiuti, M. Polanyi, Trans. Faraday Soc. 30 (1934) 1164–1172.